Earth and Planetary Science Letters 449 (2016) 282–294

Contents lists available at ScienceDirect

Earth and Planetary Science Letters

www.elsevier.com/locate/epsl

Decoupling of modern shortening rates, climate, and topography in the Caucasus

Adam M. Forte [a,*], Kelin X. Whipple [a], Bodo Bookhagen [b], Matthew W. Rossi [c]

[a] School of Earth and Space Exploration, Arizona State University, United States
[b] Institute of Earth and Environmental Science, Universität Potsdam, Germany
[c] Environmental Sciences, Northwestern University, United States

ARTICLE INFO

Article history:
Received 26 February 2016
Received in revised form 28 May 2016
Accepted 9 June 2016
Available online 21 June 2016
Editor: A. Yin

Keywords:
tectonics
erosion
climate
dynamic topography
orogenic processes

ABSTRACT

The Greater and Lesser Caucasus mountains and their associated foreland basins contain similar rock types, experience a similar two-fold, along-strike variation in mean annual precipitation, and were affected by extreme base-level drops of the neighboring Caspian Sea. However, the two Caucasus ranges are characterized by decidedly different tectonic regimes and rates of deformation that are subject to moderate (less than an order of magnitude) gradients in climate, and thus allow for a unique opportunity to isolate the effects of climate and tectonics in the evolution of topography within active orogens. There is an apparent disconnect between modern climate, shortening rates, and topography of both the Greater Caucasus and Lesser Caucasus which exhibit remarkably similar topography along-strike despite the gradients in forcing. By combining multiple datasets, we examine plausible causes for this disconnect by presenting a detailed analysis of the topography of both ranges utilizing established relationships between catchment-mean erosion rates and topography (local relief, hillslope gradients, and channel steepness) and combining it with a synthesis of previously published low-temperature thermochronologic data. Modern climate of the Caucasus region is assessed through an analysis of remotely-sensed data (TRMM and MODIS) and historical streamflow data. Because along-strike variation in either erosional efficiency or thickness of accreted material fail to explain our observations, we suggest that the topography of both the western Lesser and Greater Caucasus are partially supported by different geodynamic forces. In the western Lesser Caucasus, high relief portions of the landscape likely reflect uplift related to ongoing mantle lithosphere delamination beneath the neighboring East Anatolian Plateau. In the Greater Caucasus, maintenance of high topography in the western portion of the range despite extremely low (<2–4 mm/y) modern convergence rates may be related to dynamic topography from detachment of the north-directed Greater Caucasus slab or to a recent slowing of convergence rates. Large-scale spatial gradients in climate are not reflected in the topography of the Caucasus and do not seem to exert any significant control on the tectonics or structure of either range.

1. Introduction

Topography reflects the competition between rock uplift and erosion and thus encodes information about climate, rock strength, and tectonics (e.g., Kirby and Whipple, 2012). One important open question is the extent to which climate influences the topography and internal deformation of orogens (e.g., Whipple, 2009). Numerical and experimental models of active orogens suggest potentially strong feedbacks between rainfall, tectonics and topography (e.g., Koons, 1990; Willett, 1999). However, field evidence in support of a climate–tectonic coupling is mixed. While some studies suggest robust linkages among rainfall, runoff, erosion and uplift rates, localization of structures, and topography (e.g., Dadson et al., 2003; Reiners et al., 2003; Thiede et al., 2004), others suggest minimal ability for rainfall to influence long-term erosion rates or deformation patterns within an orogen (e.g., Burbank et al., 2003; Godard et al., 2014; Riebe et al., 2001). One reason clear identification of climatic influences on the tectonic history of orogens is challenging is because of the different time scales over which climate and tectonic changes occur and the potential for significant cross correlation (e.g., orographic precipitation concentrating rainfall in areas of high relief) (e.g., Whipple, 2009).

The Caucasus ranges in the north-central Arabia–Eurasia collision zone are an understudied, young (<10 Ma) orogenic system that provides an excellent opportunity to explore potential

* Corresponding author.
E-mail address: aforte@asu.edu (A.M. Forte).

http://dx.doi.org/10.1016/j.epsl.2016.06.013
0012-821X/

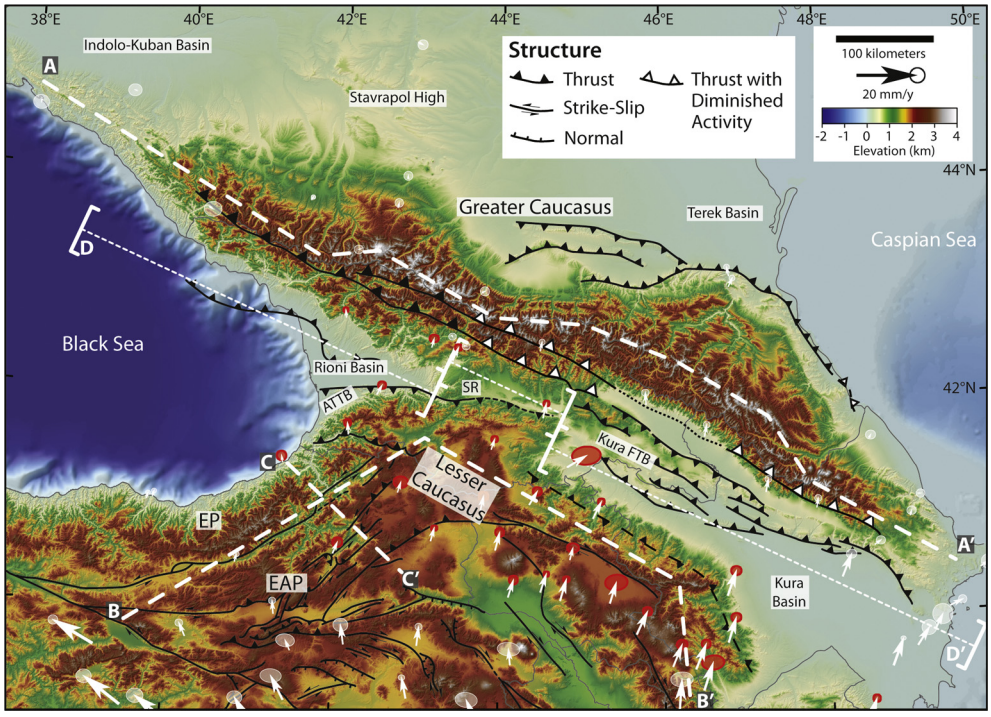

Fig. 1. Shaded relief map of the Caucasus region colored by elevation with main geologic and physiographic features labels. Topography is from 90-meter resolution Shuttle Radar Topography Mission (SRTM) data and bathymetry is from the 30-arc-second General Bathymetric Chart of the Oceans (GEBCO). Abbreviations are SR: Surami Range, ATTB: Achara-Trialet thrust belt, EP: Eastern Pontides, EAP: East Anatolian Plateau, Kura FTB: Kura fold-thrust belt. Also shown are GPS velocity vectors, relative to stable Eurasia (Kadirov et al., 2012; Reilinger et al., 2006), stations with red error ellipses (1-sigma) are within the Lesser Caucasus block used for calculating total convergence within the GC (e.g., Fig. 3). Grey lines are country borders; white lines are cross-section lines for Fig. 3 (A–A′) and Fig. 4 (B–B′ and C–C′). Major structural systems of the region. Greater Caucasus structure is from Forte et al. (2014) and Lesser Caucasus, Eastern Pontide, and Eastern Anatolia structures are from Dhont and Chorowicz (2006) and Koçyiğit et al. (2001). (For interpretation of the references to color in this figure, the reader is referred to the web version of this article.)

links between tectonics and climate. The Caucasus consists of two closely spaced, roughly parallel, east–west striking orogenic systems: (1) the Greater Caucasus (GC) and (2) the Lesser Caucasus (LC) (Fig. 1). Both orogens contain broadly similar rock types and experience a 3- to 4-fold eastward decrease in mean annual precipitation (Borisov, 1965). However, the two ranges are characterized by different tectonic regimes that allow for an opportunities to isolate effects of climate and tectonics. The extent to which the pronounced climatic gradient affects the topography or tectonics of either the GC or LC is unknown. There is an apparent disconnect between the GC topography and both climate and active shortening. In the simplest scenarios, higher convergence rates lead to wider orogens and greater relief, and greater erosivity leads to narrower orogens and lower relief (e.g., Whipple and Meade, 2004). In the GC, topographic metrics like local relief, mean elevation, and range width are similar along-strike despite the order of magnitude eastward increase in convergence rates determined from GPS velocity data and a moderate gradient in mean annual precipitation (e.g., Forte et al., 2014). Thus, in stark contrast to observations, modern gradients predict a wide, high relief orogen in the east and a narrow, low relief orogen in the west. Several mechanisms could explain the apparent disconnect between these expectations and reality. With respect to climate, the relationship between mean annual rainfall and erosivity may be complex. For example, (1) small rainfall events often do not generate enough runoff to incise into bedrock (e.g., Molnar et al., 2006) and thus mean rainfall may be a poor proxy for the geomorphically effective climate; and (2) base-level in this region is intimately linked with the history of the Caspian Sea, which experienced a partially climate driven 1–1.5 km base-level drop between 5.5 and ∼3.0 Ma (Forte and Cowgill, 2013) that possibly drove increased exhumation of portions of the Caucasus draining into the Caspian (e.g., Ballato et al., 2015). With respect to tectonics, there may be an additional source of uplift in the western GC due to (1) slab detachment (Mumladze et al., 2015) or delamination (Ershov et al., 2003); and/or (2) an along-strike change in the accretion rate or crustal structure within the GC (Forte et al., 2014). Climatic and tectonic mechanisms make distinct predictions in terms of the spatial distribution of metrics of topography, climate, and uplift and erosion rates throughout the Caucasus regions. In this contribution, we quantify some of these metrics in the Caucasus region by comparing available geologic data with several remotely-sensed datasets and historical hydro-climatic records. We attempt to reconcile the apparent disconnect between the topography and modern climatic and tectonic gradients in the GC by considering the rates of uplift and/or accretion necessary to maintain the observed topography of the range (both height and width) and use them to inform estimates of the spatial distribution of uplift and erosion rates.

2. Background

2.1. Tectonic setting

Within the central portion of the Arabia–Eurasia collision zone, NE–SW directed convergence between Arabia and Eurasia is partitioned between (1) extension and lateral escape within the East Anatolian Plateau, Lesser Caucasus (LC), and Eastern Pontides (EP) and (2) compression within the Greater Caucasus (GC) (Fig. 1, Allen et al., 2004; Reilinger et al., 2006). East–west oriented extension within the East Anatolian Plateau, LC, and EP is accommodated by conjugate strike-slip faulting and minor normal faulting (Dhont and Chorowicz, 2006; Koçyiğit et al., 2001) whereas compression within the GC is accommodated via ENE–WSW oriented thrust faults (Fig. 1, Allen et al., 2004). The majority of active shortening structures within the GC are along the margins of the range

and within the forelands (Forte et al., 2013) but the interior of the GC is still experiencing active uplift (Avdeev and Niemi, 2011; Forte et al., 2014; Mosar et al., 2010).

The GC are characterized by along-strike gradients in modern shortening rates, structural geometries, lithology, and crustal structure. Modern NE–SW convergence rates between the LC and Eurasia, inferred from GPS velocity data, increase eastward between the Black and Caspian Seas from ∼2 to ∼14 mm/y (Kadirov et al., 2012; Reilinger et al., 2006). The GC accommodate all of this convergence (Fig. 1). Whether variations in convergence rate observed in decadal GPS velocities are broadly translatable to geologic timescales is unclear. At least in the eastern GC, there is evidence that GPS velocities and average shortening rates over the 1–2 M.a. are similar (e.g., Forte et al., 2013). West of 45°E, the GC are a structurally simple, single sided, south-directed orogenic wedge, lacking a significant fold-thrust belt (Forte et al., 2014). Basement is exposed in the western GC (Fig. 2b) and the GC lack a subducted slab or significant underthrusting (Mumladze et al., 2015). In contrast, east of 45°E the GC lack exposure of basement (Fig. 2b) and are largely a two-sided orogenic wedge (Forte et al., 2014; Mosar et al., 2010) characterized by well-defined foreland fold-thrust belts (Fig. 1, Forte et al., 2013; Mosar et al., 2010) and are underlain by a north dipping subducted slab extending to at least 160 km depth (Mumladze et al., 2015). Thermochronometric data suggest more rapid uplift of ∼1 mm/y in the center of the range, with slower rates of exhumation as low as 0.1 mm/y along the tips (Avdeev, 2011; Avdeev and Niemi, 2011; Král and Gurbanov, 1996; Vincent et al., 2011). However, data is concentrated in the western GC so it is unclear if this pattern continues eastward (Fig. 2c).

The Lesser Caucasus, Eastern Pontides, and East Anatolian Plateau do not exhibit as much structural variation along-strike as the GC. Strike-slip faulting and minor normal faulting dominate active deformation (Fig. 1, Dhont and Chorowicz, 2006; Koçyiğit et al., 2001). The East Anatolia Plautea is a ∼2 km high plateau lacking mantle lithosphere (Zor, 2008) after detachment or delamination of a subducted slab (Göğüş and Pysklywec, 2008; Keskin, 2003). Cenozoic volcanic deposits related to this slab delamination event (Keskin, 2003) dominate the surface geology of the East Anatolia Plateau (Fig. 2b). The division between the EP and LC is primarily a geographic one in that the geologic history and active tectonics (Dhont and Chorowicz, 2006) of the two ranges are broadly similar. Thus we consider the LC and EP as one geologic province and collectively denote them as LC-EP (Fig. 1).

2.2. Climatic setting

At a regional scale, the present-day climate of the Caucasus is dominated by westerlies and the presence of two large high pressure systems: (1) the winter Siberian High localized over Central Asia and; (2) the summer Azores High localized over Europe (Borisov, 1965; Lydolph, 1977). These two systems, especially the Siberian High, block storm systems from northern latitudes. As such, the primary source of precipitation within the Caucasus is from east-moving weather systems originating in the Black and Mediterranean Seas that subsequently produce an eastward decrease in precipitation along-strike (Lydolph, 1977).

The topography of the GC and LC-EP, along with the broad high elevation East Anatolian Plateau, strongly impacts the regional climate. The southwestern and northwestern flank of the GC and LC-EP, respectively, create an orographic barrier that together with the Siberian High, effectively stall winter storms along the Black Sea coast and lead to mean annual precipitation (MAP) >2 m/y (Borisov, 1965). In contrast, the eastern GC and the eastern interior of the East Anatolian Plateau and LC-EP are more arid with a MAP of <0.5 m/y. The areal extent of both modern and Last Glacial Maximum (LGM) glaciation similarly decreases eastward, driven primarily by the decrease in precipitation as there are no significant along-strike changes in either elevation (Fig. 1) or temperature (Supplemental Fig. 1, Gobejishvili et al., 2011).

3. Methods

To test how climate, tectonics, and topography are related within the Caucasus region, we focus on topographic metrics known to correlate with erosion rates. We supplement topographic analysis with estimates of long term (10^6 y) erosion rates from a synthesis of published low temperature thermochronometer ages. We also analyze remotely-sensed rainfall and historic runoff records to assess whether trends in rainfall and runoff variability plausibly produce eastward increases in erosional efficiency. Erosional efficiency is the rate constant that dictates the steady-state topography for a given erosion rate. A gradient in erosional efficiency could explain the invariant relief observed along-strike if eastward increasing modern convergence rates led to increased uplift rates that were in turn counter-balanced by an increase in erosional efficiency.

3.1. Topographic metrics

In the absence of spatially continuous estimates of either long term exhumation rates or erosion rates, we use established relationships among topographic metrics and erosion rate observed in other settings (e.g., Kirby and Whipple, 2012; Lague, 2013) to assess the extent to which significant along-strike gradients in erosion rate exist within the Caucasus region. In doing this, we make the testable assumption that the topography is in an approximate steady state where erosion balances rock uplift at the scale of individual drainage basins (e.g., Willett and Brandon, 2002). Toward this end, we calculate several topographic metrics using the SRTM 90 m digital elevation model (http://srtm.csi.cgiar.org) for which established empirical relationships exist between these metrics and erosion rates. Specifically, we use (1) local relief (e.g., Ahnert, 1970; DiBiase et al., 2010), (2) catchment-mean normalized channel steepness (k_{sn}, e.g., Lague, 2013; Ouimet et al., 2009), and (3) catchment-mean hillslope angle (S_{avg}, e.g., Montgomery and Brandon, 2002; Portenga and Bierman, 2011). Local relief is the difference between minimum and maximum elevations within a specified distance and is strongly correlated with erosion rate (e.g., Ahnert, 1970; Montgomery and Brandon, 2002). We use a radius of 5 km for calculating relief that has been shown to correlate with mean k_{sn} in other settings (DiBiase et al., 2010). Local relief at this scale captures tributary channel relief and is important for potential climate–tectonic interactions because ∼1–1.5 km of relief is necessary to initiate a strong orographic effect and focusing of rainfall (e.g., Bookhagen and Burbank, 2006).

We modify an analysis presented by Ouimet et al. (2009) where empirical relations between S_{avg} and k_{sn} with catchment-mean erosion rates (determined from cosmogenic ^{10}Be in alluvial sands) were used to explain spatial variations in erosion rate from the topography alone. In an area for which catchment-mean erosion rate data does not exist, as in the Caucasus, combining S_{avg} and k_{sn} for a large number of widely distributed watersheds can be used to infer relative variations in erosion rates by incorporating both the channel profile (k_{sn}) and hillslope (S_{avg}) response to local differences in erosion rates.

For channels, erosion rate (E) and k_{sn} are related (e.g., Lague, 2013), such that:

$$E = K(k_{sn})^n \tag{1}$$

where K is the erosional efficiency and n is the slope exponent in the well known stream power river incision model (see Supple-

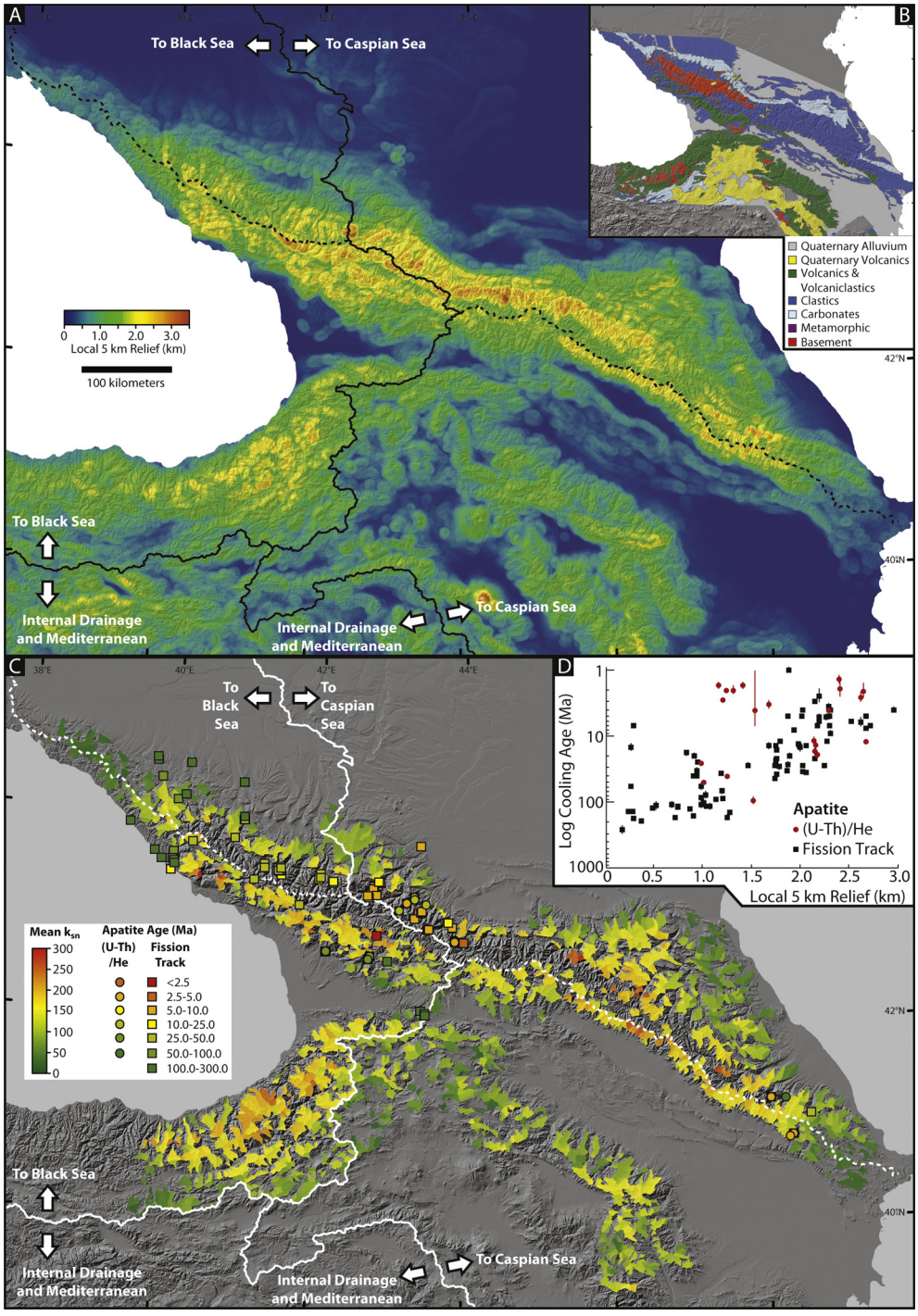

Fig. 2. A) Local relief measured in a 5-km radius moving window. Solid black lines indicate major drainage divides separating portions of the landscape draining toward the Caspian or Black Seas or toward the Mediterranean or local internal drainage and dashed lines separate rivers draining north or south within the GC. B) Simplified lithologic map of the Caucasus region. Input data is primarily the geologic map presented in Forte et al. (2014) and supplemented with geologic maps of eastern Turkey (see Supplement). C) Mean basin channel steepness for selected basins within the Greater and Lesser Caucasus, excluding portions of the GC effected by LGM glaciation, along with a synthesis of available apatite (U-Th)/He and apatite fission track data. Color scale for cooling ages is scaled that same color indicates same nominal exhumation rate assuming a 60 °C and 110 °C closure temperature for the (U-Th)/He and Fission Track data, respectively. D) Relationships between cooling ages and local 5 km relief, notice cooling ages are on a log scale and plotted with decreasing age in the positive y direction. See main text and supplemental text for additional discussion of data processing and sources. Supplemental Tables 1 and 2 contain all data associated with measured basins within the Greater and Lesser Caucasus, respectively, including basins excluded during the filtering process to remove basins with significant knickpoints not displayed here.

mental Material). The erosional efficiency parameter incorporates effects of climate and substrate properties whereas different values of n likely reflect a change in erosional process or runoff variability (Whipple, 2004; Lague, 2013).

For the hillslopes, we use two equations to define a relationship between catchment mean hillslope angle and erosion rate. The first is a 1-D analysis assumed to characterize a representative hillslope length for a catchment using an expression from

Roering et al. (2007) for hillslope elevation (z) as a function of horizontal distance (x) from the divide:

$$z(x) = \frac{-S_c^2}{2\beta E}\left[\sqrt{D^2 + (2\beta Ex/S_c)^2} - D\ln\left(\frac{\sqrt{D^2 + (2\beta Ex/S_c)^2} + D}{2\beta E/S_c}\right)\right] \quad (2)$$

where $\beta = (\rho_r/\rho_s)$, ρ_r and ρ_s are the bulk densities of rock and sediment, S_c is a limiting gradient, and D is a diffusivity coefficient. Catchment-mean hillslope angle (as a gradient) is then described by:

$$S_{avg} = \frac{z(0) - z(L_H)}{L_H} \quad (3)$$

where L_H is a characteristic hillslope length (Ouimet et al., 2009) We solve for L_H to explicitly examine the relative roles of the erosional efficiency of hillslopes (D) and rivers (K) on steady-state catchment topography (see Supplementary Material). We discuss relationships between topographic metrics and erosion rates primarily in terms of just three of the parameters from Eqs. (1), (2), and (3); K, S_c, and D. If the fluvial (K) and hillslope (D, S_c) processes are influenced by climate and lithology differently, then relating mean k_{sn} and S_{avg} at the orogen scale will reflect the influence of either climate or lithology on topography. However, if values of K, D, and, to a lesser extent, S_c co-vary as a function of climate, lithology, or both, then these plots may not be diagnostic, as illustrated below. However, we also show that these plots are still useful to describe spatial patterns in relative erosion rates. A more detailed discussion of theory relating erosion rates with k_{sn} and S_{avg} and related equations are provided in the Supplementary Material.

To apply this technique to the Caucasus, we first select individual watersheds that are at the same spatial scale as prior studies that showed robust relationships among cosmogenically derived catchment-mean erosion rates and topographic metrics (e.g., DiBiase et al., 2010; Godard et al., 2014; Ouimet et al., 2009), namely watersheds with drainage area of ~10–100 km^2, that lack significant knickpoints, and have uniform lithology, climate, and k_{sn}. We employ a semi-automated process to select and filter out potentially non-equilibrium watersheds (those with significant knickpoints) and then calculate topographic metrics (see Supplemental Material). Areas of the topography affected by LGM glaciation were removed and thus excluded from the analysis (Supplemental Fig. 1).

3.2. Modern climate

While regional climate patterns within the Caucasus are well established (e.g., Borisov, 1965; Lydolph, 1977), it is notoriously difficult to capture spatial patterns of rainfall in steep topography from ground-station data alone. We use satellite data from the Tropical Rainfall Measurement Mission (TRMM) 3B42 V7 collected from 1998–2012 (e.g., Bookhagen and Burbank, 2006) to explore rainfall gradients within the Caucasus region. TRMM data has been successfully used in other mountainous settings to better characterize spatial gradients in rainfall, rainfall variability, and the frequencies of extreme rainfall events (e.g., Boers et al., 2013). These kinds of data provide the spatial detail that is needed for erosion studies (e.g., Bookhagen and Burbank, 2006). The TRMM 3B42 data has a footprint of ~30 × 30 km (0.25 × 0.25 degree) and a 3-hour temporal resolution, which we use to calculate (1) mean daily rainfall, (2) ratio of wet to dry days (where a wet day is defined a day with >0.01 mm rainfall), and (3) fraction of the average annual rainfall delivered in the five largest events per year at each grid cell. We supplement the TRMM analysis with several higher spatial resolution MODIS datasets including daily land surface temperature (MOD11A1, 1 × 1 km), 8-day averages of snow cover (MOD10C2, ~6 × 6 km), and 16-day averages of the enhanced vegetation index (EVI, MOD13A2′, 1 × 1 km) for the time span of 2002–2012. Details of the processing of this data along with an expanded analysis are presented in the Supplemental Material.

3.3. Runoff

Runoff generation is the link between climatological parameters and river erosion. For bedrock channels, thresholds set by the dominant incision process, bedload size, and substrate properties (e.g., Whipple, 2004) influence which flood magnitudes do geomorphic work. Thus, recent studies have emphasized the importance of describing the probability distribution of floods along with erosion thresholds to interpret long-term erosion rates and river profiles (e.g., Lague et al., 2005; Molnar et al., 2006; Rossi et al., 2016). Under this view, and depending on how mean runoff is related to event-scale runoff variability, it is possible that arid settings can be more erosive than more humid settings (e.g., Molnar, 2001).

In the Caucasus region, there is an increase in aridity from west to east that may also correspond to important gradients in runoff variability that may help explain the apparent disconnect between topography and mean rainfall patterns. To assess this, we acquired daily discharge data for 32 river basins in both the GC and LC from the Global Runoff Data Centre (http://www.bafg.de/GRDC). While 2 of these gauges have daily records spanning several decades, the majority of stations only operated between 1978 and 1988 (Supplemental Table 3). Daily discharge values were normalized by drainage area to calculate specific daily runoff. For each station, we calculated mean runoff and the event magnitude exceeding the 99% probability threshold. To quantify variability, we determined the best-fit shape parameter (C_R) of the stretched exponential distribution that fits observed floods exceeding the 99% probability threshold (see Supplementary Material, Rossi et al., 2016).

4. Results

4.1. Topographic metrics

Local relief (5-km radius) within the GC does not vary systematically along-strike (Fig. 2a). The highest relief (>2 km) is found in two zones, one coincident with topographic crest of the range and the other along the drainage divide, which lies up to 40 km south of the crest (Fig. 2a, Forte et al., 2014). Local relief in the LC-EP is not as continuous, with the highest relief localized in the portion draining to the Black Sea in the transitional area between the EP and LC. The rest of the LC and East Anatolian Plateau are very low relief (Fig. 2a). Bedrock geology (Fig. 2b) potentially explains patterns in relief (Fig. 2a) in the LC-EP and East Anatolian Plateau as low-relief portions of the landscape are coincident with the extent of late Cenozoic volcanic rocks. In contrast, lithologic controls on relief in the GC are not apparent (Fig. 2).

Catchment-mean k_{sn} is linearly related to local relief, as expected from results in other settings (Supplemental Fig. 4, DiBiase et al., 2010). The highest k_{sn} values in the GC are clustered near the center of the range at higher elevations (Fig. 3a). Although k_{sn} varies along- and across-strike (Fig. 3), it shows no systematic difference between basins draining toward the Caspian or Black Seas (Fig. 3b) which is inconsistent with the idea that large magnitude base-level fall of the Caspian sea is a primary driver of exhumation patterns in the Caucasus (e.g., Ballato et al., 2015). In fact, LC-EP catchment-mean k_{sn} for rivers draining to the Black Sea are significantly higher than those draining to the Caspian (Figs. 2c and 4b). In the western GC, basins south of the topographic crest

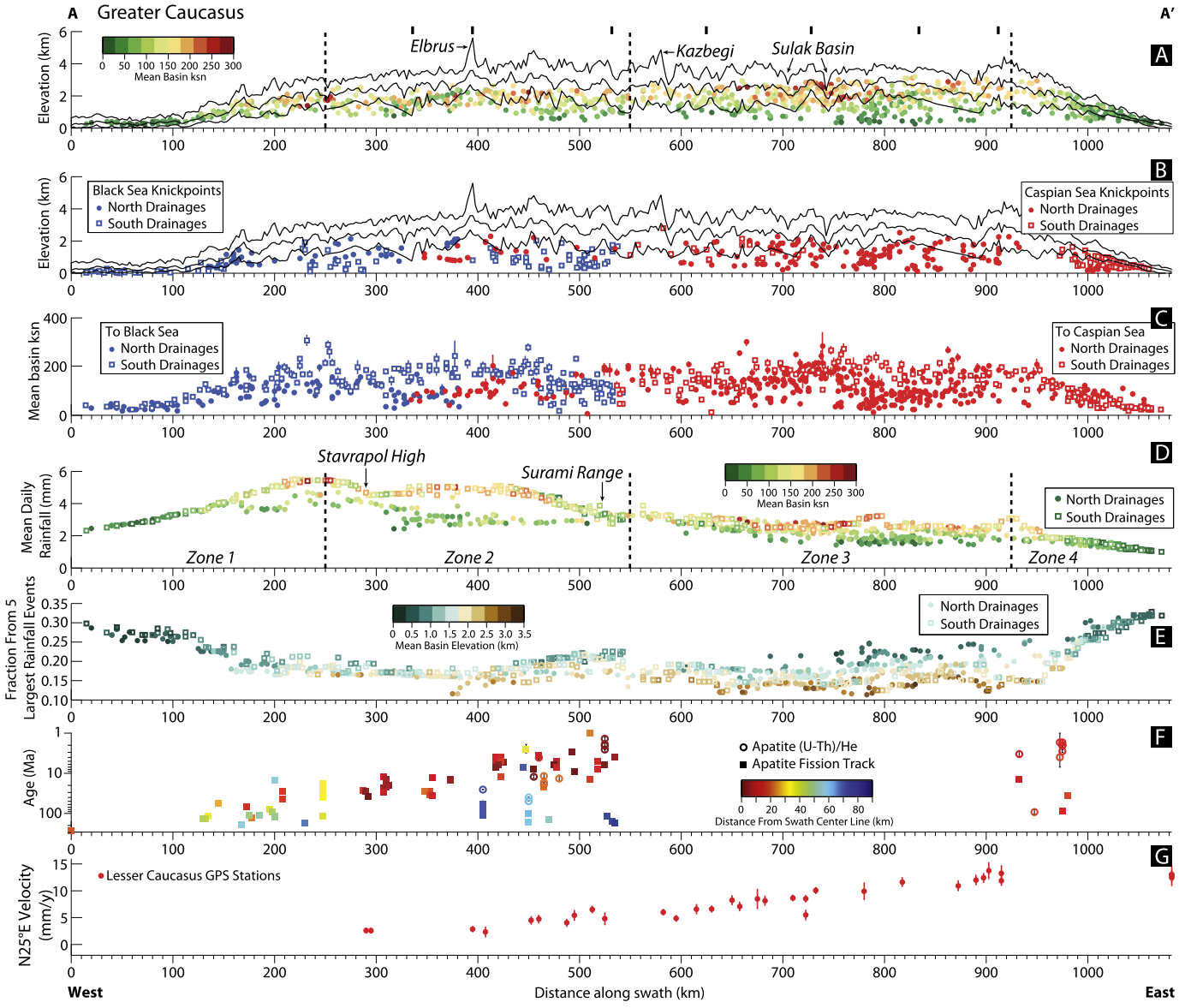

Fig. 3. Swath profiles along the crest of the Greater Caucasus (A–A′ in Fig. 1). Vertical black tick marks above panels A are locations of bends in the swath profile. A) Black lines are maximum, mean, and minimum elevations along a 20-km wide swath profile A–A′. Dots are locations of measured basins (Fig. 2c) located by projecting the centroid of the basin onto the swath profile and using the mean elevation of the basin. Basins are colored by the mean channel steepness. B) Location of knickpoints identified by individual inspection of 2nd order streams, colored by whether the rivers drain to the Black or Caspian seas. This is after knickpoints associated with contacts or LGM glaciation were removed (Supplemental Fig. 3). C) Mean channel steepness and along strike distance of basin centroids with whiskers for the standard error on this measurement. Data is colored by whether the basin drains toward the Caspian or Black Sea and flows south or north. D) Along-strike position of basins and mean daily precipitation within each basin, colored by mean channel steepness. Open squares are basins south of the topographic crest and filled circles are basins north of the crest. E) Along-strike position of basins and fraction of mean total rainfall delivered in the 5 largest events within each basin, colored by mean basin elevation. F) Ages of apatite (U-Th)/He in open circles and apatite fission track in closed squares, with locations projected onto the swath profile. Symbols are colored by distance from the swath line, measured perpendicular to the swath line, which we use to approximate distance from the topographic crest of the range. G) N25E components of LC-EP GPS velocity measurements relative to stable Eurasia projected onto the swath profile line.

have higher mean k_{sn} than those north of the crest. In contrast, the eastern GC show no clear difference between northern or southern basins (Fig. 3c). This observation is consistent with the distribution of major active structures (Fig. 1) and was previously interpreted to reflect an along-strike eastward transition between a singly-vergent, south-directed orogen to a doubly-vergent orogen (Forte et al., 2014).

4.2. Rainfall

Mean daily rainfall patterns from TRMM 3B42 and those inferred from MODIS data are consistent with previous regional syntheses from ground-based station data (e.g., Borisov, 1965; Lydolph, 1977), but add important detail. The principal feature is a pronounced eastward decrease in rainfall throughout the Caucasus region (Figs. 3d, 4c, and Supplemental Fig. 5a and d). The TRMM data indicate that the western GC imposes an orographic focusing of precipitation that is the most pronounced in the foreland with the Rioni Basin receiving >1.8 m/y of rain while the Indol-Kuban Basin receives <0.7 mm/y (Supplemental Fig. 5a). While the interior of the southwestern GC are measurably wetter than the northwestern flank, this difference rarely exceeds 0.365 mm/y and difference between the north and south flanks become indistinguishable eastward (Fig. 3d).

We use the average fraction of total annual rainfall occurring in the 5 largest rainfall events each year (Supplemental Fig. 5c) as a

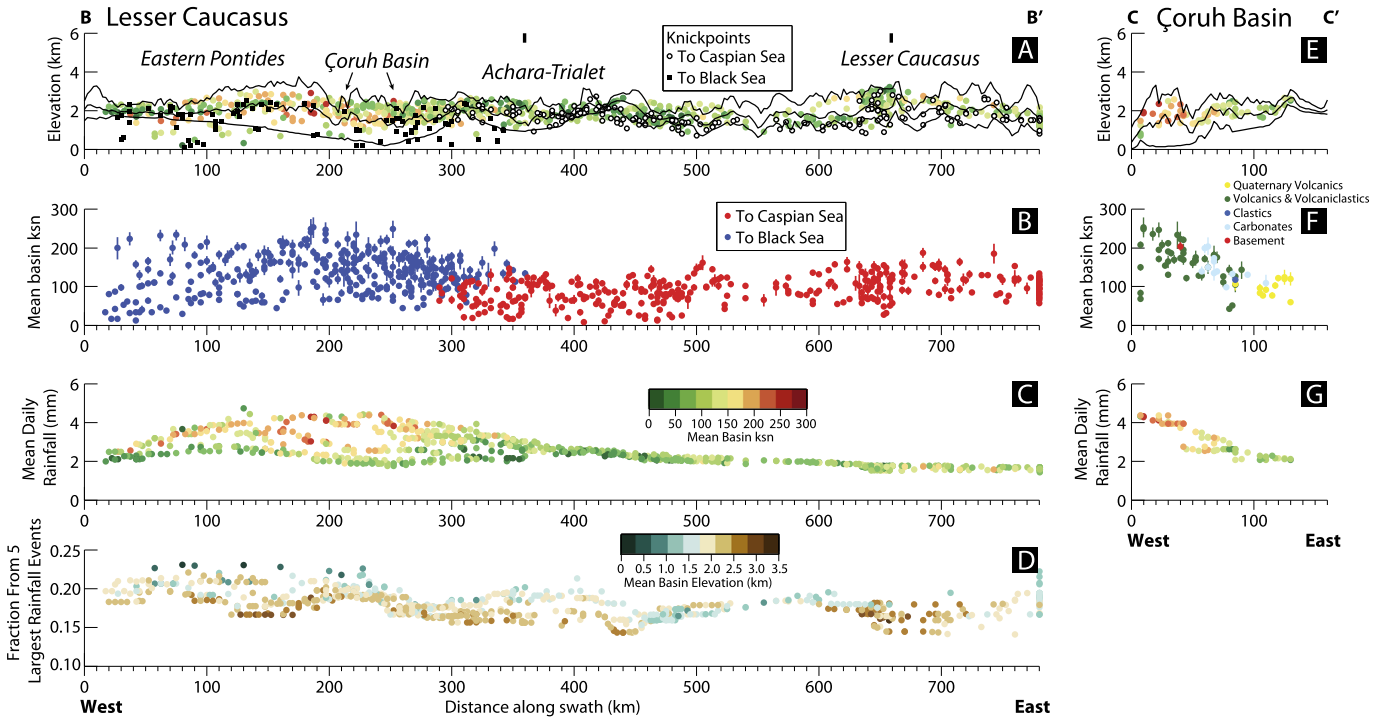

Fig. 4. Swath profiles along the crest of the Lesser Caucaus (B–B′ in Fig. 1 and panels A–D) and across the high relief portion of the Chourh river basin in the LC (C–C′ in Fig. 1 and panels E–G). Vertical black tick marks above panels A are locations of bends in the LC swath profile. A) Maximum, mean and minimum elevations for the Lesser Caucasus with measured basins (Fig. 2c) within this range. Construction of this panel is identical to that of Fig. 3A, but using profile line B–B′ (Fig. 1) Black squares and white circles indicate positions of knickpoints on rivers draining to the Black and Caspian Seas respectively. B) Mean channel steepness within the Lesser Caucasus basins colored by whether they drain to the Black or Caspian Seas. C) Mean daily precipitation within basins in the Lesser Caucasus colored by mean channel steepness. D) Along-strike position of basins and fraction of mean total rainfall delivered in the 5 largest events within each basin, colored by mean basin elevation. E) Maximum, mean, and minimum elevations across the Choruh basin along C–C′ (Fig. 1) with k_{sn} of basins within 30 km of the profile line. F) Mean k_{sn} as a function of distance, colored by dominant lithology. G) Mean MDP as a function of distance, colored by mean k_{sn}.

proxy for the event-scale rainfall variability. This fraction does not change significantly along-strike and is correlated with elevation in both the GC (Fig. 3e) and LC-EP (Fig. 4d). At high elevations in both the GC and LC-EP, large magnitude rainfall events generally represent less than 15–20% of total rainfall, whereas at lower elevations, and especially at the tips of the GC, these infrequent events may represent up to 35% of total yearly precipitation (Fig. 3e). Similarly, the ratio of wet to dry days, which is a proxy for the frequency of rainfall (Supplemental Fig. 5b) is largely invariant along-strike in both the GC and LC-EP.

4.3. Runoff

As expected, patterns in mean daily runoff throughout the Caucasus region largely mirror patterns in mean daily rainfall (Supplemental Fig. 6a). Variability in runoff, quantified as C_{rR}, does not show any systematic variation along-strike and variability is low throughout (Fig. 5a). The magnitude of 99th% events similarly mirror gradients in mean daily runoff and rainfall (Supplemental Fig. 6b). Lower variability basins often drain higher elevations, which have high standard deviations of mean monthly fraction of snow cover (Fig. 5b). High standard deviations suggest high amounts of seasonal snow cover, and consequently high amounts of runoff from snow melt. The correspondingly high values of C_R (low variability) are consistent with previous results suggesting regions that receive significant fractions of precipitation as snow tend to have lower runoff variability (e.g., Pitlick, 1994; Rossi et al., 2016).

5. Analysis and integration of datasets

Our analysis examines several datasets. Before discussing the implications of our results on the Caucasus, it is useful to synthesize how topographic metrics and exhumation rates from prior studies can best be integrated to interpret along-strike variations in erosion rates.

5.1. Inferring erosion rates from topographic metrics

In order to interpret plots of topographic metrics in the Caucasus, Figs. 6a and 6b show how theoretical changes in fluvial erosional efficiency (K), diffusivity (D), and limiting gradient (S_c), and erosion rates can alter empirical relationships between S_{avg} and k_{sn} (for more detailed discussion see Supplementary Material, equations S4, S5, S6, and S7). The following rules of thumb can be helpful when interpreting plots in Fig. 6: (1) moving along a given curve to higher values of both k_{sn} and S_{avg} implies an increase in erosion rate; (2) higher K/D ratios imply S_{avg} is more sensitive to erosion rate; (3) conversely, lower K/D ratios imply greater sensitivity of k_{sn} to erosion rates; (4) order-of-magnitude changes in K result in more substantial changes in the S_{avg}–k_{sn} relationship than do order-of-magnitude changes in D; and (5) increases in S_c shift curves to higher values of S_{avg} (Figs. 6a, b and Supplemental Material). However, two important caveats emerge: (1) similar pairings of S_{avg} and k_{sn}, can arise with different combinations of D, K, and S_c and thus imply significantly different erosion rates (Fig. 6a); and (2) co-variation of D and K (e.g., a 5 fold increase of both) produces no change in topography, but does imply a significant increase in erosion rate for a given topography (Fig. 6b). These caveats highlight the necessity for quantitative measures of erosion rate for a given landscape to calibrate values of K, D, and S_c and to assess how these quantities may vary as a function of climate and lithology. Nevertheless, such plots are still useful for exploring relative variations in erosion rate within a landscape or between landscapes as we do for the GC and LC-EP below.

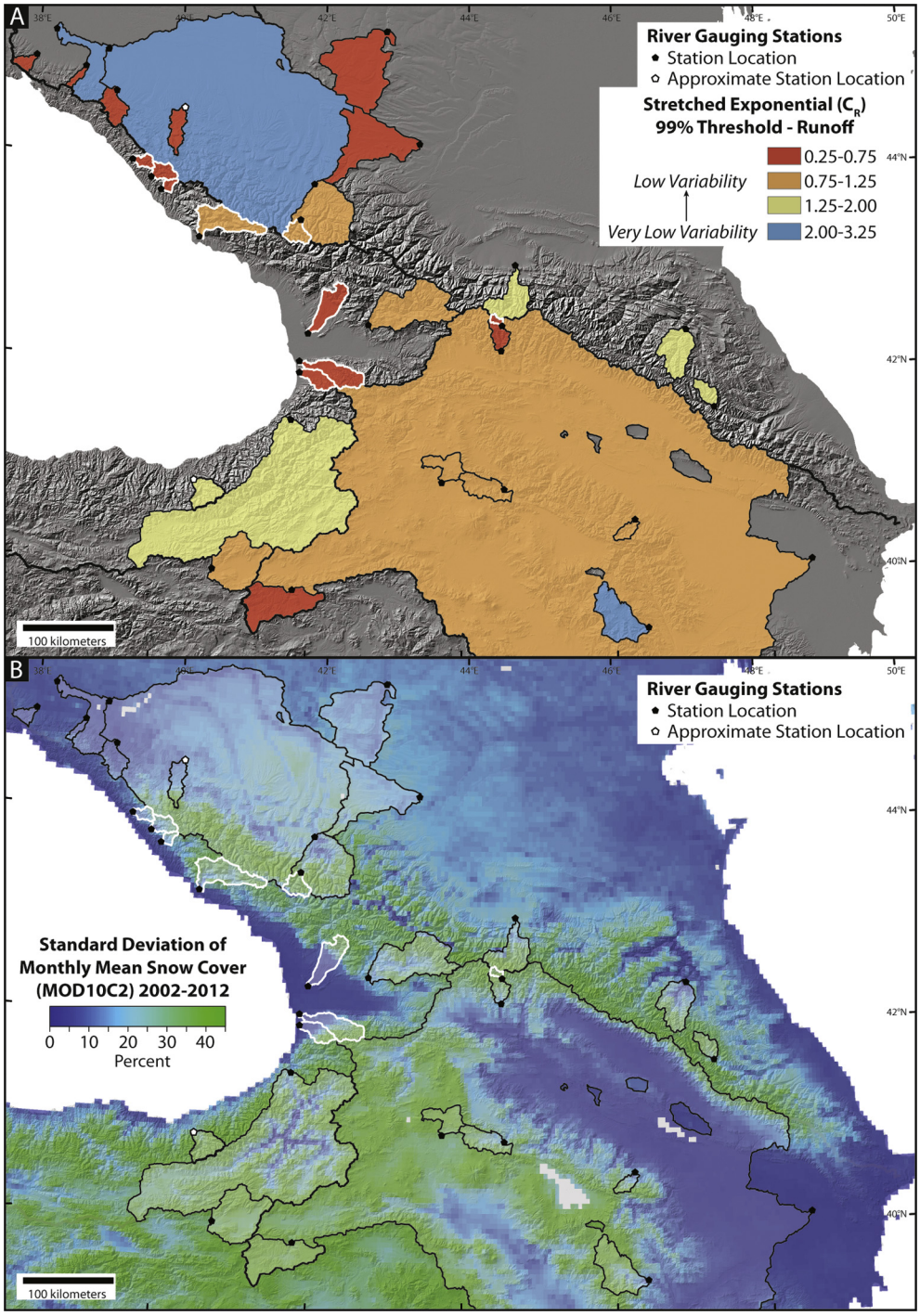

Fig. 5. Runoff data from 32 gauged basins in the Caucasus region (Supplemental Table 3). Outlines of basins are shown and location of gauging stations are shown with hexagons. Black hexagons are gauging stations for which basin outlines were provided by the Global Runoff Data Centre and white hexagons are basins for which we processed the drainage basin due to erroneous location data for the gauging station, see Supplemental Text for discussion. Basins outlined in white have a runoff ratio >1, see Supplemental Text for discussion. A) Shape parameter C_R from the stretched exponential fit of runoff events exceeding the 99% probability threshold; see main and supplemental text for discussion. B) Basin outlines and the standard deviation of monthly means of snow cover percentage from MOD10C2, areas with high standard deviations are inferred to have significant contributions of snow melt to total runoff.

S_{avg} and k_{sn} values of LC-EP basins do not vary systematically with catchment-mean basin elevation (Fig. 6e), distance along-strike, or mean daily precipitation (Supplemental Fig. 10). There is a potential weak relationship with lithology within the LC-EP, where a majority of lower S_{avg} and k_{sn} basins are associated with young volcanics forming low relief surfaces (Fig. 6f). For other lithologies, there is no clear relationship between lithology and topography.

GC catchment-mean hillslope gradient and channel steepness values show a positive trend with mean basin elevation, suggesting erosion rates increase with elevation within the GC (Fig. 6c), but there is no clear relation between lithology and topography within the GC (Supplemental Fig. 11). Taken en-masse, Fig. 6d shows that there are no clear relationships among S_{avg}, k_{sn}, and position along-strike measured relative to the swath profile (proxy for modern shortening rate) other than the low values of S_{avg} and

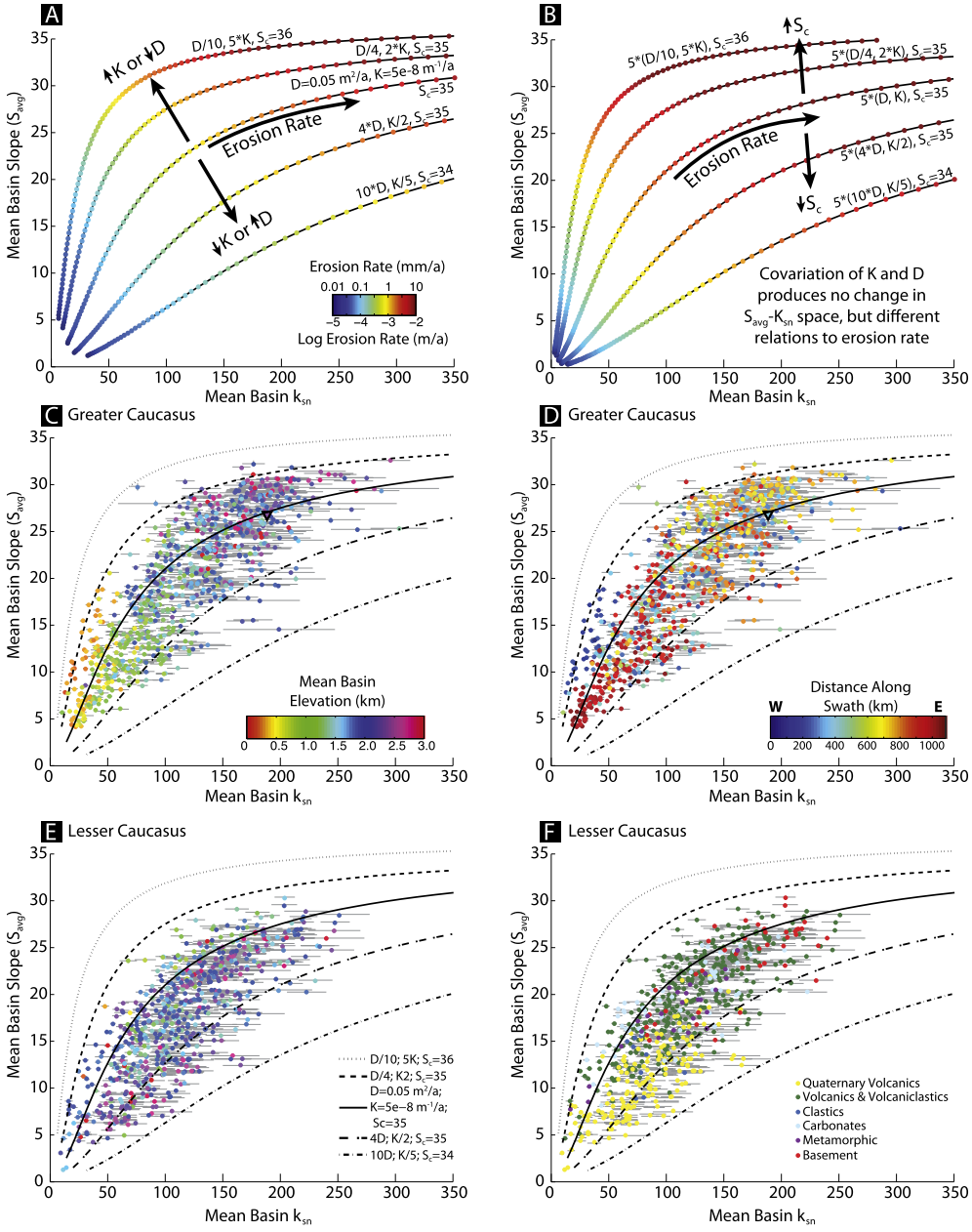

Fig. 6. Relations between catchment-mean channel steepness and catchment-mean slope. A) A series of theoretical curves constructed from combining equations (1), (2), and (3) to explore how variations in erosional efficiency (K), diffusivity (D), and critical gradient (S_c) are represented in S_{avg}–k_{sn} space. Colored dots are erosion corresponding erosion rates. See also Supplemental Fig. 8. B) Same as A but with a uniform multiplication of both K and D by 5. See also Supplemental Fig. 9. C) S_{avg}–k_{sn} data from the Greater Caucasus, colored by mean basin elevation. Data is taken from basins shown in Fig. 2b. Whiskers indicate standard errors. The single triangle represents the topographic parameters for a basin with a cosmogenic nuclide erosion rate of 1.1 +/− 0.3 mm/y from the Inguri river in the southwestern GC (Vincent et al., 2011). It is important to note however that this erosion rate is difficult to interpret with respect to topography because the sampled catchment is 1–2 orders of magnitude larger than the basins considered in our analysis (~2,800 km^2), includes significant portions of the landscape that experienced LGM glaciation, and has several large knickzones. Curves are the same as in A and B for reference. D) Greater Caucasus slope–k_{sn} data colored by distance along the swath profile line A–A′ (Fig. 1). E) Lesser Caucasus slope–k_{sn} data colored by mean basin elevation, same color scale as C. F) Lesser Caucasus slope–k_{sn} data colored by dominant lithology (e.g., Fig. 2b). See Supplemental material for additional plots.

k_{sn} observed at the tips of the range where elevations and local relief decline. Dividing the GC into along-strike regions characterized by transitions in topography, k_{sn}, and mean daily rainfall (Fig. 3a) reveals a potential relation between increasing mean daily rainfall and erosion rate (Fig. 7a–d). However, there is potential for cross-correlation as mean daily rainfall and k_{sn} both increase with elevation (Fig. 7e–h), as suggested by the lack of any along-strike trend in S_{avg} and k_{sn} associated with the dominant along-strike variation in mean daily rainfall (Figs. 3, 6). Without direct quantification of K and D, it is difficult to assess the true relations between topography and climate.

5.2. Connecting topography, implied erosion rates, and thermochronometric data

Within the GC, local relief, elevations, and mean k_{sn} define a strikingly symmetric orogen along-strike (Figs. 2 and 3) despite decreasing annual precipitation eastward (Fig. 4) and increasing modern shortening rates eastward (Fig. 1, 3f). Comparison of spatial variations in local relief (Fig. 2a), mean k_{sn} and S_{avg} (Fig. 6c) with apatite (U-Th)/He and fission track cooling ages (Avdeev, 2011; Avdeev and Niemi, 2011; Král and Gurbanov, 1996; Vincent et al., 2011) suggest broadly similar patterns (Figs. 2 and 3). Furthermore, general relationships between (1) mean k_{sn} and mean local

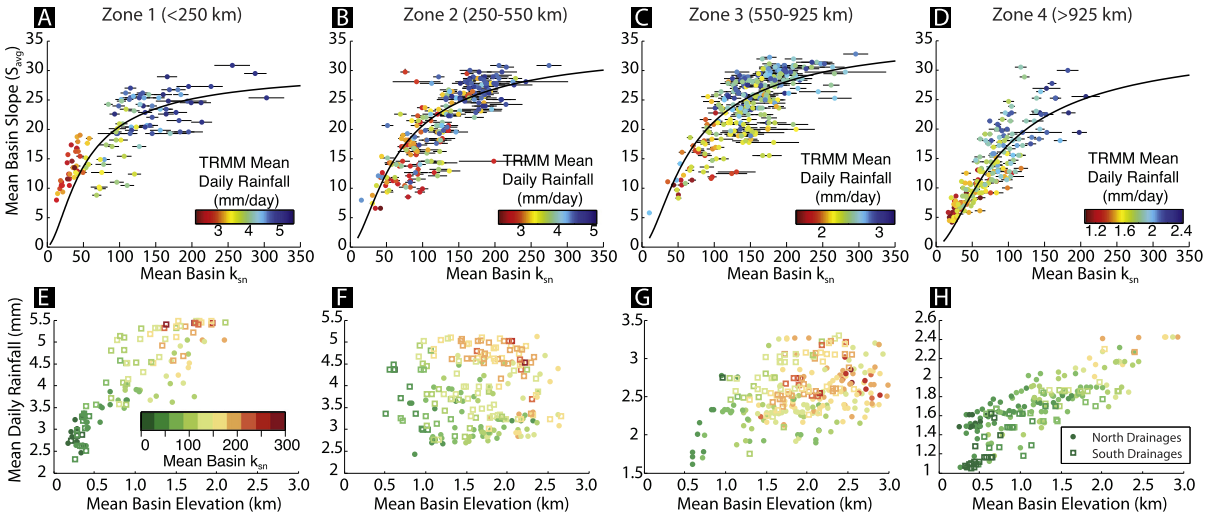

Fig. 7. Top (A–D), S_{avg}–k_{sn} data from the Greater Caucasus for four zones along the range (see Fig. 2 for division locations) colored by mean rainfall within each drainage basin. Note that the color scale changes between panels. Black line in each panel is constructed by using equations (1), (2), and (3) and varying parameters of K, D, and S_c to find a best visual fit with the data. Bottom (E–H), relation between mean basin elevation and mean daily precipitation for each of the four zones for the same drainage basins as in A–D. Data is colored by mean channel steepness and whether the basin is within a river network flowing north or south within the GC.

relief (Supplemental Fig. 4) and (2) local relief and cooling ages indicate that the correlations between inferred high erosion rates and high topography (Fig. 6 and 7) are largely reflective of long-term (10^6 y) exhumation rates (Fig. 2d). An important caveat to the use of the available thermochronologic data is that while some of this previous work was carefully conducted to explore the potential for anomalous age-elevation relationships (e.g., Avdeev and Niemi, 2011), this is not the case for all. As such, there is the potential for additional complications to the interpretations of these cooling ages that is beyond the scope of this work.

To first order, the relation between S_{avg}, k_{sn} and basin elevation suggests an increase in erosion rate with elevation throughout the GC (Fig. 6c). This is also consistent with local relief (Fig. 2) and thermochronometer ages (Figs. 2c and 3), with high relief and young thermochrometer ages at higher elevations, near the center of the orogen, which imply more rapid erosion. In contrast, the flanks and tips of the GC have low relief, low k_{sn} (Fig. 2), and relatively old thermochronometer ages (Figs. 2c and 3). In detail, this relationship is most robust for the western GC where there are abundant thermochronometer ages, but the general correlations between topographic metrics and the cooling ages imply a similar pattern throughout the orogen (Fig. 2d).

6. Discussion

We next consider the implications of our results and our preliminary analysis for the connections between topography, climate, and tectonics within the Caucasus region.

6.1. The Lesser Caucasus and Eastern Pontides (LC-EP)

Our analysis of the topography of the LC-EP is largely consistent with previous work suggesting that the high topography of the region is driven by the aesthenospheric upwelling beneath the East Anatolian Plateau (Dhont and Chorowicz, 2006; Koçyiğit et al., 2001), but reveals some interesting subtleties. The most prominent feature within the LC-EP is the high relief region along the Black Sea coast of the LC-EP, localized within and near the Choruh river basin (Fig. 2). Because there is no apparent relation between k_{sn} and rock type here (Fig. 4f), this is mostly easily explained as localization of active uplift. The high relief region is notable with respect to the relatively subdued topographic expression of the Lesser Caucasus' rangefront farther east (Fig. 2 and Supplemental Fig. 12). In detail, the high relief region sits atop a low seismic velocity zone within the upper mantle, interpreted as upwelling aesthenosphere driving the uplift of the EAP as a whole (Supplemental Fig. 12, e.g., Zor, 2008). The coincidence of high relief topography with the extent of the low seismic velocity suggests that the fundamental difference between the topography of the western and eastern LC results from the location of the mantle upwelling zone and proximity to base level imposing a steeper topographic gradient.

It is interesting to note that this region also represents one of the most abrupt climate gradients in the region (Fig. 4g and Supplemental Fig. 5). In detail, mean k_{sn} and mean daily rainfall are positively correlated (Fig. 4g), and thus permits a climatic influence for the localization of active uplift. However, this pattern is also expected without a climate–tectonic coupling as higher relief will drive an orographic enhancement of precipitation. As such, the driver for uplift here, and for the topography farther east in the LC, is still likely the mantle upwelling elevating the East Anatolian Plateau, though the concentration of precipitation along the western flank of the range could allow for focusing of exhumation in this region. As such, we cannot reject the potential for a climatic influence on the topography and internal partitioning of deformation within the EP.

6.2. The Greater Caucasus (GC)

We do not find robust evidence of an orogen-scale climatic influence on the topography or erosion rates within the GC. The similarity along-strike in the fraction of total rainfall from large storm events (Fig. 4c), ratio of wet to dry days (Fig. 4b), runoff variability (Fig. 5a), and the eastward decrease in the magnitude of extreme runoff events (Supplemental Fig. 6b) precludes a scenario whereby an eastward increase in shortening and uplift is balanced by a commensurate increase in erosional efficiency. In detail, the lack of a gradient in runoff or climatic variability coupled with a decrease in the mean precipitation indicates an expected eastward decrease in erosional efficiency. The lack of a difference between the topography or spatial patterns of knickpoints within the GC drained by the Caspian versus the Black Sea (Figs. 2a and 3b) also precludes a large role for differing climatically mediated base-level changes in the Caspian Sea (e.g., Forte and Cowgill, 2013) as compared to the Black Sea like the one proposed by Ballato et al. (2015).

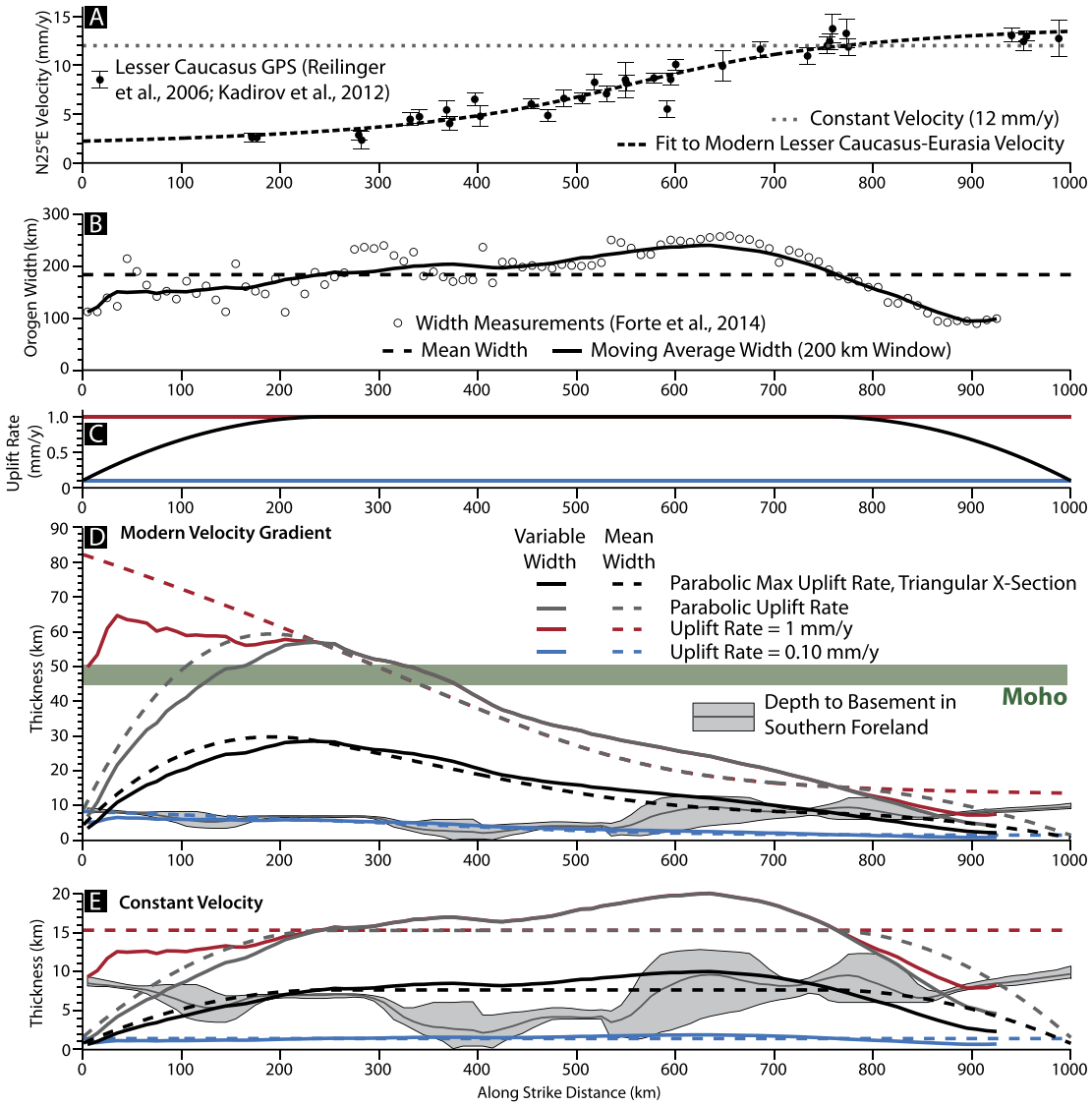

Fig. 8. Analysis of the feasibility of a gradient in accreted thickness to explain the disconnect between topography and shortening rate in the Greater Caucasus. A) Black dots are N25E velocity of Lesser Caucasus GPS stations, relative to stable Eurasia, with locations projected on profile C–C′ (Fig. 1). Dashed black line is an arctangent fit to the modern shortening rates and dotted line is a constant 12 mm/y rate. B) White dots are measures or orogen width from Forte et al. (2014), dashed black line is a mean width for the orogen from this data, and solid black line is a 200 km wide moving average of the individual width measurements. C) Four assumed uplift rates along-strike of the Greater Caucasus, constant rates of 1.0 (red) or 0.10 (blue) mm/y and a parabolic uplift rate varying between 1.0 and 0.10 mm/y that is either constant across-strike (grey) or triangular in shape across-strike (black). D) Estimates of required thickness along-strike in order for the Greater Caucasus to maintain width, using either the mean width (dashed lines) or moving average width (solid lines) the modern convergence gradient, and uplift rates from C. These thicknesses are compared to an estimate of depth to basement within the southern foreland of the Greater Caucasus from Alexidze et al. (1993), measured along a 10 km wide, broken swath D–D′ (Fig. 1) and estimates of the total crustal thickness (Zor, 2008). E) Same as D but using a constant convergence velocity of 12 mm/y. (For interpretation of the references to color in this figure, the reader is referred to the web version of this article.)

The only region where there is a plausible climatic influence on tectonics is within the southwestern GC (Zones 1 & 2, Fig. 3). Here, there appears to be a co-variation of precipitation and k_{sn}, with the highest k_{sn} values and highest rates of precipitation localized along the southwestern flank of the range, also consistent with general predictions of orographic enhancement of precipitation (Fig. 3d). However, this portion of the range is also singly vergent, with active tectonics dominated by a series of thrusts along the southern margin of the range (e.g., Forte et al., 2014). While the possibility of climate influencing location of structures in the western GC remains, the broader along-strike climatic gradient does not produce a noticeable difference in topography or long-term exhumation rates at the orogen scale suggesting that climate exerts a minimal influence.

6.3. Using accretion models to reconcile along-strike patterns in relief within the Greater Caucasus

In the absence of strong climatic forcing, we envision three primary mechanisms in which similar topography, uplift, and erosion rates along-strike could be maintained within the GC despite the gradient in modern shortening rates: (1) compensation of the westward decrease in shortening rate by a complementary increase in thickness of accreted material, (2) a temporal change in convergence rate, or (3) an additional source of uplift within the western GC related to slab detachment or crustal delamination. All of these scenarios can be considered within the context of a simple mass balance that can be applied to small, collisional orogens like the GC (e.g., Whipple and Meade, 2004). The underlying assumptions of this are that: (1) the accretionary flux into an orogen is the

product of the thickness of material entering the orogen and the rate of convergence, (2) the erosional flux is the product of the orogen width and the average uplift rate, and (3) that the orogen has approached a steady-state where the accretionary flux and erosional flux are equal (e.g., Whipple and Meade, 2004). If the GC are in mass balance, the near-constant orogen width along-strike together with the implied similarity in uplift rates from our topographic analysis, requires near constant accretion rates along-strike. Given the along-strike variation in convergence rate, near constant accretion rates could only be supported by an eastward decrease in the thickness of accreted material. The extent to which the GC are in mass balance is unknown, but long term maintenance of orogenic width is consistent with the geology of the western GC, which lacks evidence of either abandoned structures or significant propagation into the foreland (e.g., Forte et al., 2014). The eastern GC widened with the formation of the Kura fold-thrust belt ca. 2 Ma (Forte et al., 2013), but it is reasonable to assume that it has maintained its width since that time.

We test the feasibility of variable thickness of the accretionary flux along-strike by using the modern convergence gradient (Fig. 8a), measures of orogen width (Fig. 8b, Forte et al., 2014) and assuming four different uplift rate patterns. Fig. 8c shows how the maximum rate for each uplift rate pattern varies along-strike, with either a constant uplift rate of 1 mm/y, a constant uplift rate of 0.10 mm/y, or a parabolic uplift rate varying between 0.1 and 1 mm/y along-strike. We use two different formulations of the parabolic uplift rate, one in which the velocity is constant in any across-strike section (grey line in Fig. 8d) and another in which uplift velocity has a triangular cross section with velocity going to zero at the margins of the range (black line in Fig. 8d). These different scenarios are used to solve for the necessary thickness of material accreted into the GC to maintain width (Fig. 8d, Whipple and Meade, 2004). The 0.10 and 1 mm/y constant uplift rates represent minimum and maximum uplift rates, respectively, from thermochronologic data (Avdeev, 2011; Avdeev and Niemi, 2011; Král and Gurbanov, 1996; Vincent et al., 2011). The two parabolic uplift gradients are representative of the gross shape of the relief structure within the GC and are consistent with relations between the topography and long term uplift rates (e.g., Fig. 2d). We compare calculated thicknesses with estimates of depth to basement along a 10-km wide swath profile through the southern foreland (Fig. 1 and Supplemental Fig. 13, Alexidze et al., 1993). While the actual thickness of material accreted into the GC is not constrained by these data, the depth to basement serves as a useful reference. For the low-convergence western GC, both high constant uplift rates and parabolic uplift rates scenarios require thicknesses significantly larger than the depth to basement, and in many cases, greater than the total crustal thickness of the region (Fig. 8d, e.g., Zor, 2008). At constant low uplift rates, the required thickness is within the measured depth to basement, but this average rate is too low to explain the available thermochronometer data.

If we instead assume that modern shortening is not representative of the past and use a constant shortening rate of 12 mm/y (Fig. 8a), the required thicknesses for all scenarios are reasonable. The parabolic uplift rate with triangular cross-section scenario falls mostly within the depth-to-basement throughout the profile (Fig. 8e). This analysis suggests that accretion at the modern convergence rates is sufficient for the eastern GC, but not for the western GC. In other words, if the western GC is maintaining its width then accretion is insufficient to generate the uplift rates that characterize the region. However, if past convergence rates were faster, then accretion models may explain the western GC. Geologic rates of shortening in the western GC are unconstrained, and thus we cannot evaluate this scenario at present.

If, however, the modern convergence gradient is representative of the past, which is argued to be the case for the region since ∼5 Ma (e.g., Allen et al., 2004), an additional uplift mechanism is required for the western GC. Subcrustal structure of the western GC indicates that a mechanism may exist in the form of dynamic topography related to either slab detachment (Mumladze et al., 2015) or crustal delamination (Ershov et al., 2003). We cannot resolve between these two with our data, but slab detachment is the simpler explanation. Slab detachment allows for a period of faster convergence rates in the western GC that is driven by slab pull prior to detachment followed by an additional source of vertical uplift after detachment. Models of slab detachment predict enhanced rates of uplift following detachment, localized in a narrow region, ∼100 km, above the detachment point, though the exact location and geometry of the resultant surface uplift will depend on the location and the depth of the detachment point (e.g., Göğüş and Pysklywec, 2008). Fully evaluating the feasibility of either the change in shortening rate or slab detachment hypotheses ultimately requires additional geophysical data along with more comprehensive estimates of erosion and shortening rates throughout the range.

7. Conclusions

We conducted a detailed hydroclimatic analysis of satellite-derived rainfall and gauging-station-derived discharge data to better characterize modern climate gradients within the Greater and Lesser Caucasus and found that mean precipitation and runoff each decrease eastward, and that variability in both precipitation and runoff remains similar. Both mean climate and event-scale variability argue for an eastward decrease in erosional efficiency that is not observed in a corresponding change in topography. For instance, despite the inferred reduction in erosional efficiency that is also coincident with an increase in convergence rates within the Greater Caucasus, the expected increase in topographic relief is not observed. Estimates of relative changes in erosion rates from topographic metrics along with syntheses of thermochronologic ages suggest relatively similar rates of erosion and uplift along-strike. Additionally, the topography appears to largely reflect long-term rates of uplift and erosion, in opposition to strong gradients in plate convergence rate and climate. If the modern eastward increasing shortening rate within the Greater Caucasus is representative of geologic rates, then simple accretion of material into the range is insufficient to explain the high relief topography or measured cooling ages of the western Greater Caucasus. Thus, we hypothesize that an additional, primarily vertical component of uplift, likely related to slab detachment beneath this portion of the range, is partially responsible for maintaining topography in the western Greater Caucasus. This additional dynamic topography is not necessarily required if past rates of convergence within the western Greater Caucasus were comparable to modern rates in the eastern Greater Caucasus.

In the Lesser Caucasus, the eastward decrease in erosional efficiency does correspond to a change to more subdued, low relief topography, but this is opposite from simple predictions of climatic influence on topography. Instead, this change in topography along-strike is more likely driven by increasing distance from the aesthenospheric upwelling driving uplift within the East Anatolian Plateau and western Lesser Caucasus and eastern Pontides. Results from both the Lesser and Greater Caucasus highlight the potential for isostatic uplift related to slab detachment and/or delamination to dramatically influence the topography of active orogens.

Finally, considering the relative importance of climate or tectonics in shaping the topography of the Greater and Lesser Caucasus suggests generally that tectonics is the principle driver of topography in this region. While we cannot completely discount local coupling between high rates of orographically-focused precipitation and apparent localization of structures or more active

uplift in the southwestern Greater and northwestern Lesser Caucasus, the difference between larger-scale, along-strike changes in topographic metrics between the two ranges, in spite of relatively similar climatic gradients, serves to highlight the dominance of the decidedly different tectonic regimes of the two orogens.

Acknowledgements

We thank the Global Runoff Data Centre, 56068 Koblenz, Germany and the European Climate Assessment and Dataset for providing runoff and precipitation station data, respectively. We thank an anonymous reviewer for input that improved this manuscript. This work was supported by National Science Foundation grant EAR-1450970 to AMF and KXW.

Appendix A. Supplementary material

Supplementary material related to this article can be found online at http://dx.doi.org/10.1016/j.epsl.2016.06.013.

References

Ahnert, F., 1970. Functional relationships between denudation, relief, and uplift in large mid-latitude drainage basins. Am. J. Sci. 268, 243–263.
Alexidze, M.A., Gugunava, G.E., Kiria, D.K., Chelidze, T.L., 1993. A three-dimensional stationary model of the thermal and thermoelastic fields of the Caucasus. Tectonophysics 227, 191–203.
Allen, M.B., Jackson, J., Walker, R., 2004. Late Cenozoic reorganization of the Arabia–Eurasia collision and the comparison of short-term and long-term deformation rates. Tectonics 23. http://dx.doi.org/10.1029/2003TC001530.
Avdeev, B., 2011. Tectonics of the Greater Caucasus and the Arabia–Eurasia Orogen. Geological Sciences, The University of Michigan.
Avdeev, B., Niemi, N.A., 2011. Rapid Pliocene exhumation of the central Greater Caucasus constrained by low-temperature thermochronometry. Tectonics 30.
Ballato, P., Landgraf, A., Fox, M., Stockli, D.F., Schildgen, T.F., Ghassemi, M.R., Kirby, E., Strecker, M.R., 2015. The growth of a mountain belt forced by base-level fall: tectonics and surface processes during the evolution of th Alborz Mountains, N. Iran. Earth Planet. Sci. Lett. 425, 204–218.
Boers, N., Bookhagen, B., Marwan, N., Kurths, J., Marengo, J., 2013. Complex networks identify spatial patterns of extreme rainfall events of the South American Monsoon. Geophys. Res. Lett. 40.
Bookhagen, B., Burbank, D., 2006. Topography, relief, and TRMM-derived rainfall variations along the Himalaya. Geophys. Res. Lett. 33, L08405.
Borisov, A.A., 1965. Climates of the U.S.S.R. Oliver & Boyd, Edinburgh and London.
Burbank, D., Blythe, A.E., Putkonen, J., Pratt-Sitaula, B., Gabet, E., Oskin, M., Barros, A., Ojha, T.P., 2003. Decoupling of erosion and precipitation in the Himalayas. Nature 426, 652–655.
Dadson, S.J., Hovius, N., Chen, H., Dade, W.B., Hsieh, M.-L., Willett, S.D., Hu, J.-C., Horng, M.-J., Chen, M.-C., Stark, C.P., Lague, D., Lin, J.-C., 2003. Links between erosion, runoff variability and seismicity in the Taiwan orogen. Nature 426, 648–651.
Dhont, D., Chorowicz, J., 2006. Review of the neotectonics of the Eastern Turkish–Armenian Plateau by geomorphic analysis of digital elevation model imagery. Int. J. Earth Sci. 95, 34–49.
DiBiase, R.A., Whipple, K.X., Heimsath, A.M., Ouimet, W.B., 2010. Landscape form and millennial erosion rates in the San Gabriel Mountains, CA. Earth Planet. Sci. Lett. 289, 134–144.
Ershov, A.V., Brunet, M.-F., Nikishin, A.M., Bolotov, S.N., Nazarevich, B.P., Korotaev, M.V., 2003. Northern Caucasus basin: thermal history and synthesis of subsidence models. Sediment. Geol. 156, 95–118.
Forte, A.M., Cowgill, E., 2013. Late Cenozoic base-level variations of the Caspian Sea: a new review of its history and proposed driving mechanisms. Palaeogeogr. Palaeoclimatol. Palaeoecol. 386, 392–407.
Forte, A.M., Cowgill, E., Murtuzayev, I., Kangarli, T., Stoica, M., 2013. Structural geometries and magnitude of shortening in the eastern Kura fold-thrust belt, Azerbaijan: implications for the development of the Greater Caucasus Mountains. Tectonics 32.
Forte, A.M., Cowgill, E., Whipple, K.X., 2014. Transition from a singly vergent to doubly vergent wedge in a young orogen: the Greater Caucasus. Tectonics 33, 2077–2101.
Gobejishvili, R., Lomidze, N., Tielidze, L., 2011. Late Pleistocene (Würmian) Glaciations of the Caucasus. In: Ehlers, J., Gibbard, P.L., Hughes, P.D. (Eds.), Quaternary Glaciations – Extent and Chronology. Elsevier, Amsterdam, pp. 141–147.
Godard, V., Bourles, D., Spinabella, F., Burbank, D., Bookhagen, B., Fisher, G.B., Moulin, A., Leanni, L., 2014. Dominance of tectonics over climate in Himalayan denudation. Geology.
Göğüş, O.H., Pysklywec, R.N., 2008. Mantle lithopshere delamination driving plateau uplift and synconvergent extension in eastern Anatolia. Geology 36, 723–726.
Kadirov, F., Floyd, M., Alizadeh, A., Guliev, I., Reilinger, R., Kuleli, S., King, R., Toksoz, M.N., 2012. Kinematics of the eastern Caucasus near Baku, Azerbaijan. Nat. Hazards 63, 997–1006.
Keskin, M., 2003. Magma generation by slab steepening and breakoff beneath a subduction–accretion complex: an alternative model for collision-related volcanism in Eastern Anatolia, Turkey. Geophys. Res. Lett. 30. http://dx.doi.org/10.1029/2003GL018019.
Kirby, E., Whipple, K.X., 2012. Expression of active tectonics in erosional landscapes. J. Struct. Geol. 44, 54–75.
Koçyiğit, A., Yılmaz, A., Adamia, S., Kuloshvili, S., 2001. Neotectonics of East Anatolia Plateau (Turkey) and Lesser Caucasus: implication for transition from thrusting to strike-slip faulting. Geodin. Acta 14, 177–195.
Koons, P.O., 1990. Two-sided orogen: collision and erosion from the sandbox to the Southern Alps, New Zealand. Geology 18, 679–682.
Král, J., Gurbanov, A.G., 1996. Apatite fission track data from the Greater Caucasus pre-Alpine basement. Chem. Erde 56, 177–192.
Lague, D., 2013. The stream power river incision model: evidence, theory and beyond. Earth Surf. Process. Landf.
Lague, D., Hovius, N., Davy, P., 2005. Discharge, discharge variability, and the bedrock channel profile. J. Geophys. Res. 110, F04006.
Lydolph, P.E., 1977. Climates of the Soviet Union. Elsevier Scientific Publishing Company, Amsterdam–Oxford–New York.
Molnar, P., 2001. Climate change, flooding in arid environments, and erosion rates. Geology 29, 1071–1074.
Molnar, P., Anderson, R.S., Kier, G., Rose, J., 2006. Relationships among probability distributions of stream discharges in floods, climate, bed load transport, and river incision. J. Geophys. Res. 111, F02001.
Montgomery, D.R., Brandon, M.T., 2002. Topographic controls on erosion rates in tectonically active mountain ranges. Earth Planet. Sci. Lett. 201, 481–489.
Mosar, J., Kangarli, T., Bochud, M., Glasmacher, U.A., Rast, A., Brunet, M.-F., Sosson, M., 2010. Cenozoic-recent tectonics and uplift in the Greater Caucasus: a perspective from Azerbaijan. In: Sosson, M., Kaymakci, N., Stephenson, R.A., Bergerat, F., Starostenko, V.I. (Eds.), Sedimentary Basin Tectonics from the Black Sea and Caucasus to the Arabian Platform. Geological Society, London, pp. 261–280.
Mumladze, T., Forte, A.M., Cowgill, E., Trexler, C.C., Niemi, N.A., Yikilmaz, M.B., Kellogg, L.H., 2015. Subducted, detached, and torn slabs beneath the Greater Caucasus. GeoResJ 5, 36–46.
Ouimet, W.B., Whipple, K.X., Granger, D.E., 2009. Beyond threshold hillslopes: channel adjustment to base-level fall in tectonically active mountain ranges. Geology 37, 579–582.
Pitlick, J., 1994. Relation between peak flows, precipitation, and physiography for five mountain regions in the western USA. J. Hydrol. 158, 219–240.
Portenga, E.W., Bierman, P.R., 2011. Understanding Earth's eroding surface with ^{10}Be. GSA Today 21, 4–10.
Reilinger, R., McClusky, S., Vernant, P., Lawrence, S., Ergintav, S., Cakmak, R., Ozener, H., Kadirov, F., Guliev, I., Stepanyan, R., Nadariya, M., Hahubia, G., Mahmoud, S., Sakr, K., ArRajehi, A., Paradissis, D., Al-Aydrus, A., Prilepin, M., Guseva, T., Evren, E., Dmitrotsa, A., Filikov, S.V., Gomez, F., Al-Ghazzi, R., Karam, G., 2006. GPS constraints on continental deformation in the Africa–Arabia–Eurasia continental collision zone and implications for the dynamics of plate interactions. J. Geophys. Res. 111. http://dx.doi.org/10.1029/2005JB004051.
Reiners, P.W., Ehlers, T.A., Mitchell, S.G., Montgomery, D.R., 2003. Coupled spatial variations in precipitation and long-term erosion rates across the Washington Cascades. Nature 426, 645–647.
Riebe, C.S., Kirchner, J.W., Granger, D.E., Finkel, R.C., 2001. Minimal climatic control on erosion rates in the Sierra Nevada, California. Geology 29, 447–450.
Roering, J.J., Perron, J.T., Kirchner, J.W., 2007. Functional relationships between denudation and hillslope form and relief. Earth Planet. Sci. Lett. 264, 245–258.
Rossi, M.W., Whipple, K.X., Vivoni, E.R., 2016. Precipitation and evapotranspiration controls on event-scale runoff variability in the contiguous United States and Puerto Rico. J. Geophys. Res. 121.
Thiede, R.C., Bookhagen, B., Arrowsmith, J.R., Sobel, E.R., Strecker, M.R., 2004. Climatic control on rapid exhumation along the Southern Himalayan Front. Earth Planet. Sci. Lett. 222, 791–806.
Vincent, S.J., Carter, A., Lavrishchev, A., Rice, S.P., Barabadze, T.G., Hovius, N., 2011. The exhumation of the western Greater Caucasus: a thermochronometric study. Geol. Mag. 148, 1–21.
Whipple, K.X., 2004. Bedrock rivers and the geomorphology of active orogens. Annu. Rev. Earth Planet. Sci. 32, 151–185.
Whipple, K.X., 2009. The influence of climate on the tectonic evolution of mountain belts. Nat. Geosci. 2, 97–104.
Whipple, K.X., Meade, B., 2004. Controls on the strength of coupling among climate, erosion, and deformation in two-sided, frictional orogenic wedges at steady state. J. Geophys. Res. 109, F01011.
Willett, S.D., 1999. Orogeny and orography: the effects of erosion on the structure of mountain belts. J. Geophys. Res. 104, 28,957–28,982.
Willett, S.D., Brandon, M.T., 2002. On steady states in mountain belts. Geology 30, 175–178.
Zor, E., 2008. Tomographic evidence of slab detachment beneath eastern Turkey and the Caucasus. Geophys. J. Int. 175, 1273–1282.